

SVasP: Self-Versatility Adversarial Style Perturbation for Cross-Domain Few-Shot Learning

Wenqian Li^{1,2}, Pengfei Fang^{1,2*}, Hui Xue^{1,2*}

¹School of Computer Science and Engineering, Southeast University, Nanjing 210096, China

²Key Laboratory of New Generation Artificial Intelligence Technology and Its Interdisciplinary Applications (Southeast University), Ministry of Education, China
{wenqianli.li, fangpengfei, hxue}@seu.edu.cn

Abstract

Cross-Domain Few-Shot Learning (CD-FSL) aims to transfer knowledge from seen source domains to unseen target domains, which is crucial for evaluating the generalization and robustness of models. Recent studies focus on utilizing visual styles to bridge the domain gap between different domains. However, the serious dilemma of gradient instability and local optimization problem occurs in those style-based CD-FSL methods. This paper addresses these issues and proposes a novel crop-global style perturbation method, called **Self-Versatility Adversarial Style Perturbation (SVasP)**, which enhances the gradient stability and escapes from poor sharp minima jointly. Specifically, SVasP simulates more diverse potential target domain adversarial styles via diversifying input patterns and aggregating localized crop style gradients, to serve as global style perturbation stabilizers within one image, a concept we refer to as self-versatility. Then a novel objective function is proposed to maximize visual discrepancy while maintaining semantic consistency between global, crop, and adversarial features. Having the stabilized global style perturbation in the training phase, one can obtain a flattened minima in the loss landscape, boosting the transferability of the model to the target domains. Extensive experiments on multiple benchmark datasets demonstrate that our method significantly outperforms existing state-of-the-art methods. Our codes are available at <https://github.com/liwenqianSEU/SVasP>.

Introduction

Deep learning models have achieved significant advancements in visual recognition when trained with abundant labeled samples. However, in many real-world applications, such as rare disease diagnosis, large training datasets with reliable annotations are not always feasible. To address this limitation, Few-Shot Learning (FSL) methods have been developed to enable models to generalize to novel classes with only a few samples per class (Snell, Swersky, and Zemel 2017; Sung et al. 2018; Feng et al. 2024b). In addition to the challenge of limited data, there is often a domain gap between the source domains and target domains in practical scenarios, which presents a critical challenge. Consequently, Cross-Domain Few-Shot Learning (CD-FSL) methods have been explored to transfer domain-agnostic knowledge from multiple well-annotated source domains to target domains with limited labeled data (Tseng et al. 2020; Guo

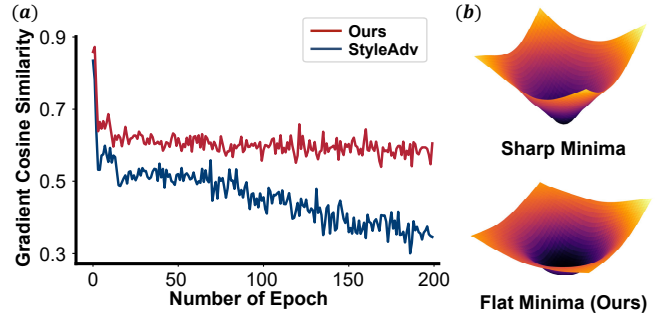


Figure 1: SVasP stabilizes the gradients and escapes from poor sharp minima. (a) demonstrates the gradient cosine similarity between epochs for displaying ground representations of gradient stability, and the larger the cosine similarity, the more stable gradient update direction. (b) demonstrates the proposed approach ensures that the model converges to a flat minima and is robust to domain shifts.

et al. 2020; Triantafillou et al. 2020; Feng, Wang, and Geng 2024). Among the various CD-FSL settings, Single Source CD-FSL addresses domain shifts more realistically by restricting the model to access only one source domain during training.

Recent studies have explored perturbing the styles of source domain images to facilitate models acquiring more domain-agnostic knowledge from a single source domain (Kim and Han 2024; Zhang et al. 2022; Wang et al. 2022; Zhong et al. 2022). By recognizing image styles (*e.g.*, mean and standard deviation) as key domain characteristics (Zhou et al. 2020), these studies aim to enhance model generalization and mitigate domain shifts by altering these domain-specific attributes (Feng et al. 2023; Xie et al. 2024). Although style-based methods have demonstrated effectiveness in Cross-Domain Few-Shot Learning (CD-FSL), they remain suboptimal due to the inherent differences between domains and the varied optimization paths for adversarial perturbations. As a result, models may overfit to noise or specific samples, becoming overly dependent on the source domain and thereby limiting their generalization capabilities.

Recently, StyleAdv (Fu et al. 2023) has addressed domain shifts by augmenting the original styles with signed style

gradients. Although effective in CD-FSL tasks, StyleAdv exhibits significant gradient instability. As illustrated in Figure 1 (a), we measure the gradient cosine similarity between the forward and backward gradients to assess gradient stability. However, we observe a continuous decline and severe oscillations in gradient cosine similarity, indicating that stable gradient optimization is unattainable. This instability is attributed to the absence of target domains and inadequate collection of gradient information from the source domain, which can misdirect adversarial style attacks (Wang and He 2021). Moreover, StyleAdv’s strategy of employing minimal perturbations for adversarial training tends to make the model overly sensitive to such perturbations, thereby undermining its robustness.

To address these challenges, we leverage diverse inputs from a single source domain to enhance style diversity and propose a novel framework called Self-Versatility Adversarial Style Perturbation (SVasP). We argue that localized crop style gradients play a crucial role in model performance. The core idea of SVasP is to enhance the transferability of source domain knowledge by integrating localized crop style gradients with global style optimization. Contrary to StyleAdv, our SVasP improves the stability of model gradient in the optimization phase, shown in Figure 1 (a). As training progresses, the issue of gradient oscillation is effectively mitigated, allowing the model to escape sharp minima and achieve smoother, flatter minima, which are more conducive to improving the model’s generalization, as illustrated in Figure 1 (b).

Specifically, our method employs a structure of inner and outer iterations. In each outer iteration, sections of the benign image are randomly cropped and resized for use in the subsequent inner iterations. During each inner iteration, we iteratively generate and integrate all crop style gradients, applying them to target the global style of the benign image. The central concept of our approach is to stabilize the gradients by incorporating as much relevant gradient information from the source domain as possible. To the best of our knowledge, this is the inaugural study exploring the impact of localized style gradients on model generalization.

The main contribution of our paper is three-fold:

- We propose a new framework called SVasP that incorporates crop style gradients with the global style gradients within a image itself, which is called self-versatility, to efficiently stabilize gradients for adversarial style attack and escape from the sharp minima.
- We design a novel objective function, named Discrepancy & Consistency Optimization (DCO) to maximize visual discrepancy between seen and unseen domains while maintaining semantic consistency.
- We conduct extensive experiments on multiple benchmark datasets and validate the effectiveness of our modules. The quantitative results show that our proposed SVasP significantly improves the model’s generalizability over other state-of-the-art(SOTA) methods.

Related Work

Cross-Domain Few-Shot Learning. Cross-Domain Few-Shot Learning (CD-FSL) aims to train a model on source domains that can effectively generalize to target domains, first introduced in (Chen et al. 2018a). Key benchmarks include BSCD-FSL (Guo et al. 2020), *mini-CUB* (Tseng et al. 2020), and Meta-Dataset (Triantafillou et al. 2020).

CD-FSL methods can be categorized based on access to target domain data: Single Source CD-FSL (Zou et al. 2024; Sun et al. 2021; Wang and Deng 2021; Hu and Ma 2022), unlabeled target-domain CD-FSL (Islam et al. 2021; Phoo and Hariharan 2021; ZHENG et al. 2023), and labeled target-domain CD-FSL (Fu, Fu, and Jiang 2021; Zhuo et al. 2022; Fu et al. 2022). This paper focuses on the most realistic and challenging setting, Single Source CD-FSL, where only a source domain dataset is accessible.

Input Diversity for Domain Shift. To address domain shift, many methods enhance input diversity. In domain generalization, MiRe (Chen et al. 2022) mixes images from different domains, and CreTok (Feng et al. 2024a) combines tokens for creative generation. In object detection, DoubleAUG (Qi et al. 2024) exchanges RGB channels, and RECODE (Li et al. 2024) decomposes visual features into subject, object, and spatial features. In CD-FSL, LDP-net (Zhou et al. 2023) extracts local features, TGDM (Zhuo et al. 2022) and meta-FDMixup (Fu, Fu, and Jiang 2021) mix source and auxiliary data, and ConFeSS (Das, Yun, and Porikli 2021) and (ZHENG et al. 2023) use different augmentation methods. These augmentation methods generate diverse input patterns and more generic features for transfer. However, none of these works consider the gradient instability problem, which is a critical issue in Single Source CD-FSL.

Gradient-based Optimization. Various gradient-based optimization methods improve model robustness and generalization. GradNorm (Chen et al. 2018b) and GAM (Zhang et al. 2023) explore gradient normalization techniques. CGDM (Du et al. 2021) minimizes the discrepancy between gradients from source and target samples. Fishr (Rame, Dancette, and Cord 2022) aligns domain-level loss landscapes by leveraging gradient covariances, and PCGrad (Yu et al. 2020) addresses conflicting gradients in multi-task learning. However, these methods often overlook diverse patterns, such as crop image style gradients, which limits their effectiveness in addressing model overfitting.

Methodology

This section introduces the proposed novel framework SVasP, designed for CD-FSL. An overview of our method is depicted in Figure 2.

Problem Formulation

We focus on the Single Source CD-FSL setting where only a source dataset \mathcal{D}^s can be accessed while the target dataset \mathcal{D}^t is forbidden. Notably, for CD-FSL, $C(\mathcal{D}^s) \cap C(\mathcal{D}^t) = \emptyset$, $P(\mathcal{D}^s) \neq P(\mathcal{D}^t)$, where $C(\cdot)$ and $P(\cdot)$ denote the categories and distributions of the source and target dataset, respectively. Moreover, episode training is used in this work.

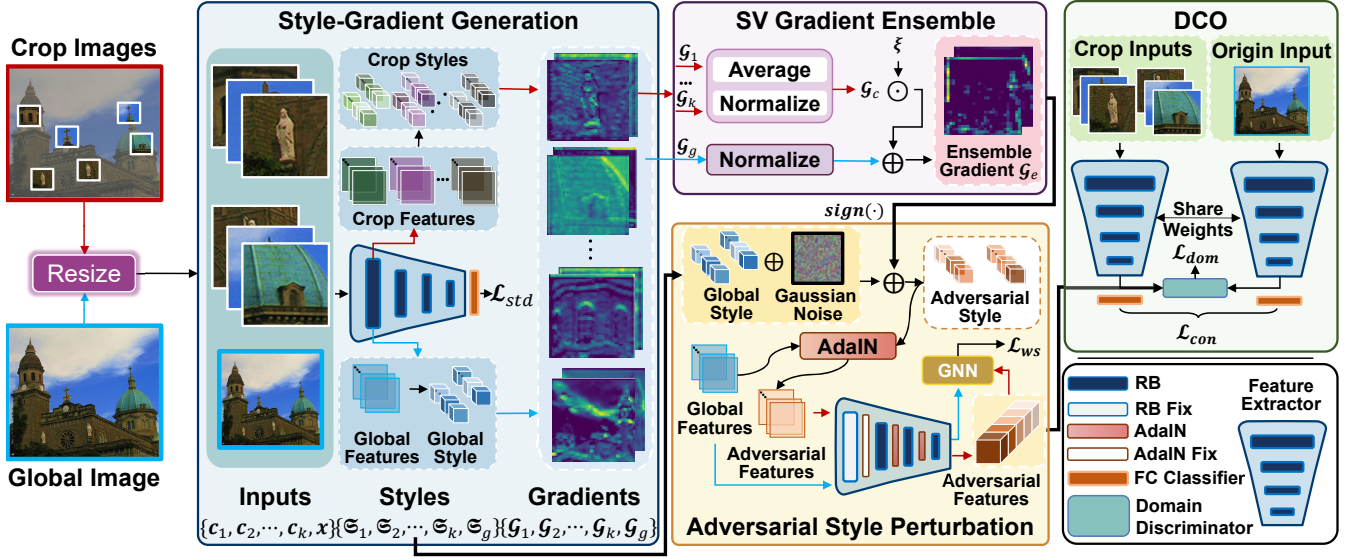


Figure 2: Overview of our proposed methods SVasP. “RB” is an abbreviation for ResNet Block. Random cropping the benign image and generates several crop images. Then, four main modules are performed: a) Generate the gradients of both crop and global styles (illustration with B_1); b) Integrate localized crop style gradients into the global style gradients; c) Perform adversarial style perturbation based on AdaIN method; d) DCO: Maximize domain visual discrepancy and global-crop consistency.

Specifically, to simulate the N -way K -shot problem, N classes are selected and K samples per class are chosen to form the support set $\mathcal{S} = \{\mathbf{x}_i^s, \mathbf{y}_i^s\}_{i=1}^{n_s}$, where $n_s = NK$. And the same N classes with another M images are used to construct the query set $\mathcal{Q} = \{\mathbf{x}_i^q\}_{i=1}^{n_q}$, where $n_q = NM$. Therefore, an episode $\mathcal{T} = (\mathcal{S}, \mathcal{Q})$ is constituted, comprising of a support set \mathcal{S} and a query set \mathcal{Q} , and $|\mathcal{T}| = N(K + M)$. The goal is to classify the images of the query set by training a feature extractor and a classification head on the support set.

SVasP

Overview. The proposed model contains a CNN/ViT backbone E , a domain discriminator f_{dom} , a global FC classifier f_g and a FSL relation classifier f_{re} with learnable parameter $\theta_E, \theta_{dom}, \theta_g$ and θ_{re} , respectively.

The network consists of four components: Style-Gradient Generation module to produce global and crop style gradients, Self-Versatility (SV) Gradient Ensemble module to integrate the localized crop style gradients as the global perturbation stabilizers, Adversarial Style Perturbation module to simulate diverse unseen styles, and Discrepancy & Consistency Optimization (DCO) to maximize the discrepancy between seen and unseen domains and maintains global-crop semantic consistency.

Without accessing auxiliary data, SVasP moderates the gradient instability and achieves a flatter minima, robustly improving the model’s generalizability. Further details are provided in the following sections.

Style-Gradient Generation. In this paper, the styles of global and crop features are modeled as Gaussian distributions (Li et al. 2022b) and learnable parameters which will

be updated by adversarial training. Specifically, for feature maps $\mathbf{F} \in \mathbb{R}^{B \times C \times H \times W}$, where B, C, H and W denote the batch size, channel, height, width of the feature maps \mathbf{F} , the specific formula for calculating the style $\mathfrak{S} = \{\boldsymbol{\mu}, \boldsymbol{\sigma}\}$ is:

$$\boldsymbol{\mu} = \frac{1}{HW} \sum_{h=1}^H \sum_{w=1}^W \mathbf{F}_{B,C,h,w}, \quad (1)$$

$$\boldsymbol{\sigma} = \sqrt{\frac{1}{HW} \sum_{h=1}^H \sum_{w=1}^W (\mathbf{F}_{B,C,h,w} - \boldsymbol{\mu})^2 + \epsilon}, \quad (2)$$

where ϵ is a small value to avoid division by zero.

Unlike directly perturbing the global style, we consider incorporating crop style gradients to stabilize the global style gradients. For each benign image and label pair (\mathbf{x}, \mathbf{y}) , we randomly crop k local images by the scale parameter $s = \{s_l, s_h\}$, where s_l and s_h denote the lower and upper bound for the area of the random cropped images respectively and get the input set $\mathbb{I} = \{c_1, c_2, \dots, c_k, \mathbf{x}\}$. Instead of generating the adversarial style of all blocks’ features at once, we use an iterative approach. Concretely, the embedding module E has four blocks B_1, B_2, B_3, B_4 , and style transformation only performs on the first three blocks, as the shallow blocks produce more migratory features. For each block B_j of the backbone E , we obtain the crop and global feature maps $\mathbb{F}^j = \{\mathbf{F}_1^j, \mathbf{F}_2^j, \dots, \mathbf{F}_k^j, \mathbf{F}_g^j\}$. For each $\mathbf{F}^j \in \mathbb{F}^j$, $\mathbf{F}^j \in \mathbb{R}^{B \times C \times H \times W}$, \mathbf{F}^j is accumulated from block 1 to block $j - 1$:

$$\mathbf{F}^j = \mathfrak{T}_j(\mathfrak{T}_{j-1}(\dots(\mathfrak{T}_1(\mathbf{I}, \mathfrak{S}_{adv}^1), \dots), \mathfrak{S}_{adv}^{j-1}), \mathfrak{S}_{adv}^j) \quad (3)$$

where transferring features between block $j - 1$ and block j

is formulated as:

$$\mathfrak{T}_j(\mathbf{F}^j, \mathfrak{G}_{adv}^j) = \frac{B_j(\mathbf{F}^{j-1}) - \boldsymbol{\mu}_{F^j}}{\boldsymbol{\sigma}_{F^j}} * \boldsymbol{\sigma}_{adv}^j + \boldsymbol{\mu}_{adv}^j \quad (4)$$

and the style $\mathfrak{G}_{F^j} = \{\boldsymbol{\mu}_{F^j}, \boldsymbol{\sigma}_{F^j}\}$ of \mathbf{F}^j is calculated by Eq. (1) and (2). Thus, we can get the styles of the feature maps of B_j to form the style set $\mathbb{S} = \{\mathfrak{G}_1^j, \mathfrak{G}_2^j, \dots, \mathfrak{G}_k^j, \mathfrak{G}_g^j\}$. Then, we continue to pass \mathbf{F}^j to the remainder of the backbone and the global FC classifier without performing any other operations and get the final prediction $\mathbf{p} = f_g(B_4(\dots(B_{j+1}(\mathbf{F}^j))); \theta_g)$, $\mathbf{p} \in \mathbb{R}^{B \times N_c}$, where N_c denotes the total number of classes. Thus the total prediction set is $\mathbb{P} = \{\mathbf{p}_1, \mathbf{p}_2, \dots, \mathbf{p}_k, \mathbf{p}_g\}$. Therefore the classification loss can be written as:

$$\mathcal{L}_{cls} = \mathcal{L}_{CE}(\mathbf{p}_g, y) + \sum_{i=1}^k \mathcal{L}_{CE}(\mathbf{p}_i, y) \quad (5)$$

where $\mathcal{L}_{CE}(\cdot, \cdot)$ denotes the cross-entropy loss.

The sequel will compute the adversarial style of block B_j , we omit the subscript j for readability and calculate the gradients of the mean $\boldsymbol{\mu}$ and the std $\boldsymbol{\sigma}$ by loss back propagation:

$$\begin{aligned} \mathbb{G}^\mu &= \{\mathfrak{G}_1^\mu, \mathfrak{G}_2^\mu, \dots, \mathfrak{G}_k^\mu, \mathfrak{G}_g^\mu\} \\ &= \{\nabla_{\boldsymbol{\mu}_1} \mathcal{L}_{cls}, \nabla_{\boldsymbol{\mu}_2} \mathcal{L}_{cls}, \dots, \nabla_{\boldsymbol{\mu}_k} \mathcal{L}_{cls}, \nabla_{\boldsymbol{\mu}_g} \mathcal{L}_{cls}\} \end{aligned} \quad (6)$$

$$\begin{aligned} \mathbb{G}^\sigma &= \{\mathfrak{G}_1^\sigma, \mathfrak{G}_2^\sigma, \dots, \mathfrak{G}_k^\sigma, \mathfrak{G}_g^\sigma\} \\ &= \{\nabla_{\boldsymbol{\sigma}_1} \mathcal{L}_{cls}, \nabla_{\boldsymbol{\sigma}_2} \mathcal{L}_{cls}, \dots, \nabla_{\boldsymbol{\sigma}_k} \mathcal{L}_{cls}, \nabla_{\boldsymbol{\sigma}_g} \mathcal{L}_{cls}\} \end{aligned} \quad (7)$$

Other blocks' style gradients can be generated likewise.

SV Gradient Ensemble. Self-Versatility (SV) Gradient Ensemble module serves as the core part of our work, dedicated to bootstrapping global style gradients by integrating localized crop style gradients. We first average and normalize the style gradients of the crops to get the aggregate crop style gradients $\mathbb{G}^c = \{\mathfrak{G}_c^\mu, \mathfrak{G}_c^\sigma\}$, where:

$$\mathfrak{G}_c^\mu = Norm\left(\frac{1}{k} \sum (\mathfrak{G}_1^\mu + \mathfrak{G}_2^\mu + \dots + \mathfrak{G}_k^\mu)\right) \quad (8)$$

$$\mathfrak{G}_c^\sigma = Norm\left(\frac{1}{k} \sum (\mathfrak{G}_1^\sigma + \mathfrak{G}_2^\sigma + \dots + \mathfrak{G}_k^\sigma)\right) \quad (9)$$

Subsequently, a decay factor ξ is introduced to finally get the ensemble style gradients $\mathbb{G}^e = \{\mathfrak{G}_e^\mu, \mathfrak{G}_e^\sigma\}$, where:

$$\mathfrak{G}_e^\mu = Norm(\mathfrak{G}_c^\mu) + \xi \odot \mathfrak{G}_c^\mu \quad (10)$$

$$\mathfrak{G}_e^\sigma = Norm(\mathfrak{G}_c^\sigma) + \xi \odot \mathfrak{G}_c^\sigma \quad (11)$$

Adversarial Style Perturbation. We get the random initialized global styles $\mathfrak{G}_{init} = \{\boldsymbol{\mu}_{init}, \boldsymbol{\sigma}_{init}\}$ by adding Gaussian noise $\mathcal{N}(0, I)$, where:

$$\boldsymbol{\mu}_{init} = \boldsymbol{\mu}_g + \varepsilon \cdot \mathcal{N}(0, I) \quad (12)$$

$$\boldsymbol{\sigma}_{init} = \boldsymbol{\sigma}_g + \varepsilon \cdot \mathcal{N}(0, I) \quad (13)$$

where ε is set to $\frac{16}{255}$. Then, the ensemble gradients are incorporated into the initialized style to get the adversarial styles $\mathfrak{G}_{adv} = \{\boldsymbol{\mu}_{adv}, \boldsymbol{\sigma}_{adv}\}$, where:

$$\boldsymbol{\mu}_{adv} = \boldsymbol{\mu}_{init} + \kappa_1 \cdot sign(\mathfrak{G}_e^\mu) \quad (14)$$

$$\boldsymbol{\sigma}_{adv} = \boldsymbol{\sigma}_{init} + \kappa_2 \cdot sign(\mathfrak{G}_e^\sigma) \quad (15)$$

Notably, κ_1 and κ_2 are chosen randomly from a given set of coefficients, which will not force a consistent change in the degree of the perturbation of $\boldsymbol{\mu}$ and $\boldsymbol{\sigma}$, making the model generate a more diverse range of styles. After obtaining the adversarial styles, style migration is performed with AdaIN method to enhance the generalizability:

$$\mathbf{F}_{adv} = \frac{\mathbf{F}_g - \boldsymbol{\mu}_g}{\boldsymbol{\sigma}_g} * \boldsymbol{\sigma}_{adv} + \boldsymbol{\mu}_{adv} \quad (16)$$

Then, the adversarial and global feature maps will together be passed to the remainder of the backbone and the FSL classifier to accomplish the N -way K -shot FSL, resulting in two predictions $\mathbf{p}_g^{fsl} \in \mathbb{R}^{B \times N_c}$ and $\mathbf{p}_{adv}^{fsl} \in \mathbb{R}^{NM \times N}$. Furthermore, we can get \mathcal{L}_{fsl} :

$$\mathcal{L}_{fsl} = \mathcal{L}_{CE}(\mathbf{p}_g^{fsl}, y_{fsl}) + \mathcal{L}_{CE}(\mathbf{p}_{adv}^{fsl}, y_{fsl}) \quad (17)$$

where $y_{fsl} \in \mathbb{R}^{NM}$ is the query samples' logical labels.

DCO. We design a novel objective function named Discrepancy & Consistency Optimization (DCO) to maximize seen-unseen domain visual discrepancy and global-crop consistency for overall features $\mathbb{F}_{all} = \{\mathbf{F}_1, \mathbf{F}_2, \dots, \mathbf{F}_k, \mathbf{F}_g, \mathbf{F}_{adv}\}$. For seen-unseen domain discrepancy maximum, we consider the global and crop features to belong to the seen domain and the generated adversarial features to belong to the unseen domain. Therefore, it is possible to make the generated adversarial features located as far away from the source domain as possible. The domain discriminator contains a dropout layer and a fully connected layer. The domain discrepancy loss is:

$$\mathcal{L}_{dom} = \sum_{\mathbf{F} \in \mathbb{F}_{all}} \mathcal{L}_{CE}(f_{dom}(\mathbf{F}; \theta_{dom}), d_F) \quad (18)$$

where $d_F \in \{0, 1\}$ is the domain label with 0 (*resp.*, 1) indicating \mathbf{F} is from the seen (*resp.*, the unseen) domain. Moreover, we enforce the semantic consistency between the global and crop features as:

$$\mathcal{L}_{con} = \sum_{i=1}^k (\lambda \mathcal{L}_{CE}(\mathbf{p}_i, \mathbf{p}_g) + (1 - \lambda) \mathcal{L}_{CE}(\mathbf{p}_i^{fsl}, y_{fsl})) \quad (19)$$

where, $\mathbf{p}_i^{fsl} = f_{re}(\mathbf{F}_i; \theta_{re})$. We use Kullback-Leibler divergence loss $KL(\cdot)$ to maximize global-adversarial consistency as:

$$\mathcal{L}_{adv} = KL(\mathbf{p}_{adv}^{fsl}, \mathbf{p}_g^{fsl}) \quad (20)$$

Then the final objective loss of **SVasP** is:

$$\mathcal{L} = \mathcal{L}_{cls} + \mathcal{L}_{fsl} + \mathcal{L}_{dom} + \mathcal{L}_{con} + \mathcal{L}_{adv} \quad (21)$$

More construction details and the complete adversarial style generation pseudo-code can be found in Appendix A.

Experiments

Datasets

Following the BSCD-FSL benchmark proposed in BSCD-FSL (Guo et al. 2020) and the *mini*-CUB benchmark proposed in FWT (Tseng et al. 2020), we use *mini*ImageNet

Table 1: Quantitative comparison to state-of-the-arts methods on eight target datasets based on ResNet-10, which is pretrained on *mini*ImageNet. Accuracy of 5-way 1-shot/5-shot tasks with 95 confidence interval are reported. “FT” with \checkmark means finetuning is used, vice versa. “Aver.” means “Average Accuracy” of the eight datasets. The optimal results are marked in **bold**.

| | Method | FT | ChestX | ISIC | EuroSAT | CropDisease | CUB | Cars | Places | Plantae | Aver. |
|--------------|--------------|-------------------|-------------------|-------------------|-------------------|-------------------|-------------------|-------------------|-------------------|-------------------|--------------|
| 1-shot | GNN | \times | 22.00±0.46 | 32.02±0.66 | 63.69±1.03 | 64.48±1.08 | 45.69±0.68 | 31.79±0.51 | 53.10±0.80 | 35.60±0.56 | 43.55 |
| | FWT | \times | 22.04±0.44 | 31.58±0.67 | 62.36±1.05 | 66.36±1.04 | 47.47±0.75 | 31.61±0.53 | 55.77±0.79 | 35.95±0.58 | 44.14 |
| | ATA | \times | 22.10±0.20 | 33.21±0.40 | 61.35±0.50 | 67.47±0.50 | 45.00±0.50 | 33.61±0.40 | 53.57±0.50 | 34.42±0.40 | 43.84 |
| | SET-RCL | \times | 22.74±0.20 | 33.33±0.40 | 65.53±0.60 | 68.43±0.50 | 46.98±0.50 | 32.84±0.40 | 56.93±0.50 | 37.43±0.40 | 45.53 |
| | StyleAdv | \times | 22.64±0.35 | 33.96±0.57 | 70.94±0.82 | 74.13±0.78 | 48.49±0.72 | 34.64±0.57 | 58.58±0.83 | 41.13±0.67 | 48.06 |
| | SVasP | \times | 23.23±0.35 | 37.63±0.58 | 72.30±0.82 | 75.87±0.73 | 49.49±0.72 | 35.27±0.57 | 59.07±0.81 | 41.22±0.62 | 49.26 |
| | ATA | \checkmark | 22.15±0.20 | 34.94±0.40 | 68.62±0.50 | 75.41±0.50 | 46.23±0.50 | 37.15±0.40 | 54.18±0.50 | 37.38±0.40 | 47.01 |
| | StyleAdv | \checkmark | 22.64±0.35 | 35.76±0.52 | 72.92±0.75 | 80.69±0.28 | 48.49±0.72 | 35.09±0.55 | 58.58±0.83 | 41.13±0.67 | 49.41 |
| | SVasP | \checkmark | 23.23±0.35 | 37.63±0.63 | 72.30±0.83 | 77.45±0.68 | 49.49±0.72 | 38.18±0.61 | 59.07±0.81 | 41.22±0.62 | 49.82 |
| | | | | | | | | | | | |
| | Method | FT | ChestX | ISIC | EuroSAT | CropDisease | CUB | Cars | Places | Plantae | Aver. |
| 5-shot | GNN | \times | 25.27±0.46 | 43.94±0.67 | 83.64±0.77 | 87.96±0.67 | 62.25±0.65 | 44.28±0.63 | 70.84±0.65 | 52.53±0.59 | 58.84 |
| | FWT | \times | 25.18±0.45 | 43.17±0.70 | 83.01±0.79 | 87.11±0.67 | 66.98±0.68 | 44.90±0.64 | 73.94±0.67 | 53.85±0.62 | 59.77 |
| | ATA | \times | 24.32±0.40 | 44.91±0.40 | 83.75±0.40 | 90.59±0.30 | 66.22±0.50 | 49.14±0.40 | 75.48±0.40 | 52.69±0.40 | 60.89 |
| | SET-RCL | \times | 25.65±0.20 | 44.93±0.40 | 83.84±0.40 | 88.11±0.30 | 68.05±0.50 | 47.95±0.40 | 76.23±0.40 | 54.70±0.40 | 61.18 |
| | StyleAdv | \times | 26.07±0.37 | 45.77±0.51 | 86.58±0.54 | 93.65±0.39 | 68.72±0.67 | 50.13±0.68 | 77.73±0.62 | 61.52±0.68 | 63.77 |
| | SVasP | \times | 26.87±0.38 | 51.10±0.58 | 88.72±0.52 | 94.52±0.33 | 68.95±0.66 | 52.13±0.66 | 77.78±0.62 | 60.63±0.64 | 65.09 |
| | Fine-tune | \checkmark | 25.97±0.41 | 48.11±0.64 | 79.08±0.61 | 89.25±0.51 | 64.14±0.77 | 52.08±0.74 | 70.06±0.74 | 59.27±0.70 | 61.00 |
| | BSR | \checkmark | 26.84±0.44 | 54.42±0.66 | 80.89±0.61 | 92.17±0.45 | 69.38±0.76 | 57.49±0.72 | 71.09±0.68 | 61.07±0.76 | 64.17 |
| | ATA | \checkmark | 25.08±0.20 | 49.79±0.40 | 89.64±0.30 | 95.44±0.20 | 69.83±0.50 | 54.28±0.50 | 76.64±0.40 | 58.08±0.40 | 64.85 |
| | NSAE | \checkmark | 27.10±0.44 | 54.05±0.63 | 83.96±0.57 | 93.14±0.47 | 68.51±0.76 | 54.91±0.74 | 71.02±0.72 | 59.55±0.74 | 64.03 |
| RDC | \checkmark | 25.48±0.20 | 49.06±0.30 | 84.67±0.30 | 93.55±0.30 | 67.77±0.40 | 53.75±0.50 | 74.65±0.40 | 60.63±0.40 | 63.70 | |
| StyleAdv | \checkmark | 26.24±0.35 | 53.05±0.54 | 91.64±0.43 | 96.51±0.28 | 70.90±0.63 | 56.44±0.68 | 79.35±0.61 | 64.10±0.64 | 67.28 | |
| SVasP | \checkmark | 27.25±0.39 | 55.43±0.59 | 91.77±0.41 | 96.79±0.26 | 72.06±0.65 | 59.99±0.69 | 78.91±0.65 | 64.21±0.66 | 68.30 | |

(Ravi and Larochelle 2017) with 64 classes as the source domain. The target domains include eight datasets: ChestX (Wang et al. 2017), ISIC (Tschandl, Rosendahl, and Kittler 2018), EuroSAT (Helber et al. 2019), CropDisease (Mohanty, Hughes, and Salathé 2016), CUB (Wah et al. 2011), Cars (Krause et al. 2013), Places (Zhou et al. 2017), and Plantae (Van Horn et al. 2018). In our Single Source CD-FSL setting, target domain datasets are not available during meta-training stage.

Implementation Details

Using ResNet-10 (He et al. 2016) as the backbone and GNN as the N -way K -shot classifier, the network is meta-trained for 200 epochs with 120 episodes per epoch. ResNet-10 is pretrained *mini*ImageNet using traditional batch training. The optimizer is Adam with a learning rate of 0.001. Additionally, using ViT-small (Dosovitskiy et al. 2020) as the feature extractor and ProtoNet (Laenen and Bertinetto 2021) as the N -way K -shot classifier, the network is meta-trained for 20 epochs with 2000 episodes per epoch. The optimizer is SGD with a learning rate of $5e-5$ and 0.001 for E and

f_{re} , respectively. ViT-small is pretrained on ImageNet1K by DINO (Caron et al. 2021). We evaluate the proposed framework during testing by average classification accuracy over 1000 episodes with a 95% confidence interval. Each class contains 5 support samples and 15 query samples. Hyperparameters are set as follows: $\xi = 0.1$, $k = 2$, $\lambda = 0.2$ and choose κ_1, κ_2 from $[0.008, 0.08, 0.8]$. The probability to perform style change is set to 0.2. The details of the finetuning are attached in Appendix A. All the experiments are conducted on a single NVIDIA GeForce RTX 3090.

Experimental Results

Comparison to SOTA methods on ResNet-10. We compare the proposed SVasP with state of the art methods with ResNet-10 as the backbone in Table 1. For a fair comparison, all the competing methods follow the single source training scheme, which is more realistic and difficult. Concretely, nine representative single source CD-FSL methods are introduced including GNN (Garcia and Bruna 2018), FWT (Tseng et al. 2020), ATA (Wang and Deng 2021), SET-RCL (Zhang et al. 2022), StyleAdv (Fu et al. 2023), Fine-tune

Table 2: Quantitative comparison to state-of-the-arts methods on eight target datasets based on ViT-small, which is pretrained on ImageNet1K by DINO. Accuracy of 5-way 1-shot/5-shot tasks with 95 confidence interval are reported.

| | Method | FT | ChestX | ISIC | EuroSAT | CropDisease | CUB | Cars | Places | Plantae | Aver. |
|--------|----------|------------|-------------------|-------------------|-------------------|-------------------|-------------------|-------------------|-------------------|-------------------|--------------|
| 1-shot | StyleAdv | ✗ | 22.92±0.32 | 33.05±0.44 | 72.15±0.65 | 81.22±0.61 | 84.01±0.58 | 40.48±0.57 | 72.64±0.67 | 55.52±0.66 | 57.75 |
| | SVASP | ✗ | 22.68±0.30 | 34.49±0.46 | 72.50±0.62 | 80.82±0.62 | 85.56±0.57 | 40.51±0.59 | 75.93±0.66 | 56.25±0.65 | 58.59 |
| | PMF | ✓ | 21.73±0.30 | 30.36±0.36 | 70.74±0.63 | 80.79±0.62 | 78.13±0.66 | 37.24±0.57 | 71.11±0.71 | 53.60±0.66 | 55.46 |
| | StyleAdv | ✓ | 22.92±0.32 | 33.99±0.46 | 74.93±0.58 | 84.11±0.57 | 84.01±0.58 | 40.48±0.57 | 72.64±0.67 | 55.52±0.66 | 58.57 |
| | SVASP | ✓ | 22.68±0.30 | 34.49±0.46 | 75.51±0.57 | 83.98±0.55 | 85.56±0.57 | 40.51±0.59 | 75.93±0.66 | 56.25±0.65 | 59.36 |
| 5-shot | Method | FT | ChestX | ISIC | EuroSAT | CropDisease | CUB | Cars | Places | Plantae | Aver. |
| | StyleAdv | ✗ | 26.97±0.33 | 47.73±0.44 | 88.57±0.34 | 94.85±0.31 | 95.82±0.27 | 61.73±0.62 | 88.33±0.40 | 75.55±0.54 | 72.44 |
| | SVASP | ✗ | 26.77±0.34 | 49.75±0.46 | 88.69±0.35 | 93.25±0.36 | 95.95±0.23 | 62.60±0.61 | 89.19±0.39 | 76.49±0.50 | 72.84 |
| | PMF | ✓ | 27.27 | 50.12 | 85.98 | 92.96 | - | - | - | - | - |
| | StyleAdv | ✓ | 26.97±0.33 | 51.23±0.51 | 90.12±0.33 | 95.99±0.27 | 95.82±0.27 | 66.02±0.64 | 88.33±0.40 | 78.01±0.54 | 74.06 |
| SVASP | ✓ | 26.77±0.34 | 51.62±0.50 | 90.55±0.34 | 96.17±0.30 | 95.95±0.23 | 66.47±0.62 | 89.19±0.39 | 78.67±0.52 | 74.42 | |

Table 3: Ablation study of the proposed method with different component combinations. ‘‘SV’’ indicates SV Gradient Ensemble module.

| Method | SV | \mathcal{L}_{dom} | \mathcal{L}_{con} | Aver. (%) |
|----------|----|---------------------|---------------------|--------------|
| Baseline | - | - | - | 62.07 |
| Proposed | ✓ | | | 62.61 |
| | ✓ | ✓ | | 63.69 |
| | ✓ | | ✓ | 64.05 |
| | ✓ | ✓ | ✓ | 65.09 |

(Guo et al. 2020), BSR (Liu et al. 2020), NSAE (Liang et al. 2021) and RDC (Li et al. 2022a). As shown, under whether setting, our method outperforms the second-best approach in terms of average accuracy with a clear margin and builds a new state of the art in the majority of domains. More precisely, under 1-shot setting on ResNet-10, SVasP performs better in all domains and surpasses the strongest competitor StyleAdv significantly by +0.59%, +3.67%, +1.36%, +1.74%, +1.00%, +0.63% on ChestX, ISIC, EuroSAT, CropDisease, CUB, Cars, respectively. Under 5-shot setting on ResNet-10, SVasP performs better in 7 out of 8 domains, and the superiority of SVasP is even larger with higher accuracy by +0.80%, +5.33%, +2.14%, +0.87%, +2.00% on ChestX, ISIC, EuroSAT, CropDisease, Cars, respectively. Despite being trained on one dataset, SVasP has good generalization ability, thus producing the optimal style-based augmentation policies for the unseen target domains.

Comparison to SOTA methods on ViT-small. To further evaluate the effectiveness of our proposed technique, we apply the proposed SVasP idea to ViT models and compare their performance over other methods on the eight datasets with ViT-small as the backbone and ProtoNet as the classi-

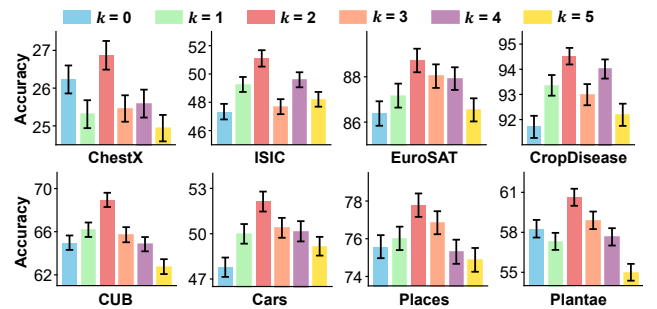


Figure 3: Performances on different numbers of crops k .

fier. As shown in Table 2, our SVasP is compared with methods like StyleAdv and PMF. SVasP achieves 58.59% and 72.84% top 1 average accuracy on either 5-way 1-shot or 5-way 5shot setting, which outperforms StyleAdv by 0.84%, 0.40%, respectively.

Qualitative Evaluation

We have performed an exhaustive and fair experimental analysis of the proposed method SVasP and the experimental results with ResNet-10 as the backbone and GNN as the classifier under the 5-way 5-shot setting are reported. More experimental results are attached in Appendix B.

Impact of different component in SVasP. To investigate the contribution of different components, we perform an ablation study on SVasP and report the result of average accuracy on eight target domains in Table 3. Specifically, we study the main technical contributions by (a) whether using SV (means the SV Gradient Ensemble module), (b) whether \mathcal{L}_{dom} and (c) whether \mathcal{L}_{con} . Among these variants, we can find that the SV Gradient Ensemble module effectively utilizes the source domain style gradients to alleviate the domain shift problem. With well constrained \mathcal{L}_{dom} and \mathcal{L}_{con} ,

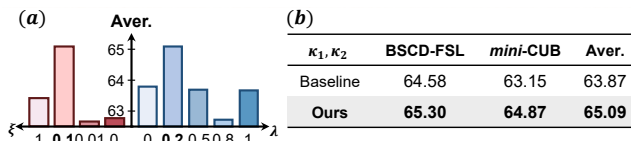


Figure 4: Performances on (a) different ξ , λ and (b) whether use same κ_1 , κ_2 . The average accuracy (%) is reported.

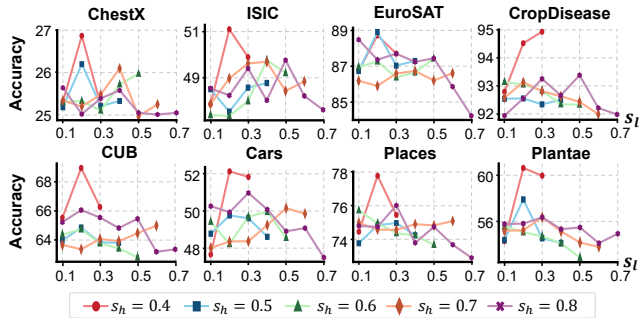


Figure 5: Performances on different scale parameters s .

SVasP improves the generalization performance and substantially improves the accuracy up to 3.02% on average.

Impact of different crop numbers k . We investigate the optimal solution for the number of crops and find that the model is most robust when the number is set to 2, as illustrated in Figure 3. Because an insufficient number of crops (*e.g.*, 0, 1) fail to represent the style gradients of the source domain and stabilize the global style perturbation. Moreover, excessive crops (*e.g.*, 3, 4, 5) can lead to overfitting of the model and limited by the source domain style.

Impact of different strategies for ξ and λ . The decay factor ξ controls the proportion of the crop style gradients that are incorporated into the global style gradients. In addition, the main component crop consistency loss \mathcal{L}_{con} has a large impact on the performance of the model, which consists of the global-crop prediction consistency loss and the crop FSL classification loss. Performances on different λ and ξ are illustrated in Figure 4 (a). As shown, the accuracy rises as ξ increase from 0 to 0.1, as the proportion increases and provides more source domain gradients. However, the accuracy decreases when the proportion is 1, as too high a proportion of the crop style gradients leads to weak global style gradients. For λ , setting the value of λ to 0.2 can realize an increase in the mean classification accuracy compared to other settings of approximately 1.62%.

Impact of different selection methods for κ_1 and κ_2 . Unlike styleadv, which sets κ_1 and κ_2 to the same value, we allow κ_1 and κ_2 to have different values to diversify the style. The experimental results verify the rationality of our setup, as shown in Figure 4 (b).

Impact of different scale parameters s . We evaluate the impact of different scale parameters s , which determines the the area of the crop images. It’s important to study optimal values of s because when the area is large, the model

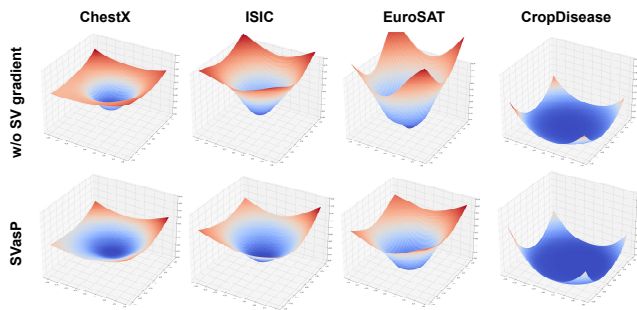


Figure 6: Loss landscape visualization results of the model without SV gradient ensemble module (first row) and our SVasP model (second row) on the BSCD-FSL benchmark.

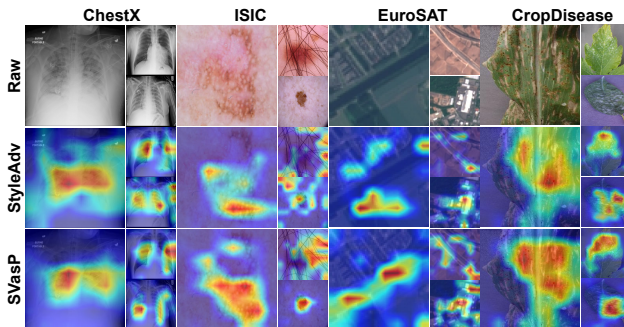


Figure 7: Grad-CAM visualization results of the StyleAdv model and our SVasP model on the BSCD-FSL benchmark. For each target dataset, three examples are demonstrated.

overlooks the local regions of inputs. We investigate the performances with $s_l \in [0.1, 0.2, 0.3, 0.4, 0.5, 0.6, 0.7]$ and $s_h \in [0.4, 0.5, 0.6, 0.7, 0.8]$, with $s_l < s_h$. The optimal result is reached when $s = (0.2, 0.4)$, as shown in Figure 5. We observe that SVasP with smaller area of crop images performs better, which demonstrates the effectiveness of our introduction of localized crop style gradients.

Visualization Results. We visualize the loss landscape following (Li et al. 2018) on the BSCD-FSL benchmark to verify the validity of our proposed important module, as shown in Figure 6. SVasP achieves a stronger flatness which can stand for the better generalization. In addition, in order to provide a more intuitive comparison about the performance of “SVasP”(ours) and “StyleAdv” model, we visualize the class-activation map using the Grad-CAM (Selvaraju et al. 2017) on the BSCD-FSL benchmark, as shown in Figure 7. We can observe that, StyleAdv may pay attention to insignificant things and is disorganized. In contrast, SVasP can focus on more key areas of the target images with the help of the localized crop style gradients. Visualization results on the *mini-CUB* benchmark can be found in Appendix C.

Conclusion

We explore the Single Source Cross-Domain Few-Shot Learning, focusing on the limitations of style-based ap-

proaches and addressing the domain shift problem. Our study introduces a novel network to capitalize on the localized crop style gradients, achieving state-of-the-art performance on both ResNet-10 and ViT-small backbone. To enhance the training process, we employ a random cropping strategy and integrate crop style gradients as the style perturbation stabilizers. This approach prevents the model from being confined to the source domain style and local loss minima. Extensive experimental results demonstrate the effectiveness and insights of the proposed method, highlighting its rationality and potential for broader application.

References

- Caron, M.; Touvron, H.; Misra, I.; Jégou, H.; Mairal, J.; Bojanowski, P.; and Joulin, A. 2021. Emerging properties in self-supervised vision transformers. In *Proceedings of the IEEE/CVF Conference on Computer Vision and Pattern Recognition*, 9650–9660.
- Chen, C.; Tang, L.; Liu, F.; Zhao, G.; Huang, Y.; and Yu, Y. 2022. Mix and reason: Reasoning over semantic topology with data mixing for domain generalization. In *Proceedings of Advances in Neural Information Processing Systems*, 33302–33315.
- Chen, W.-Y.; Liu, Y.-C.; Kira, Z.; Wang, Y.-C. F.; and Huang, J.-B. 2018a. A Closer Look at Few-shot Classification. In *Proceedings of International Conference on Learning Representations*.
- Chen, Z.; Badrinarayanan, V.; Lee, C.-Y.; and Rabinovich, A. 2018b. Gradnorm: Gradient normalization for adaptive loss balancing in deep multitask networks. In *Proceedings of International Conference on Machine Learning*, 794–803.
- Das, D.; Yun, S.; and Porikli, F. 2021. ConfeSS: A framework for single source cross-domain few-shot learning. In *Proceedings of the International Conference on Learning Representations*, 1–12.
- Dosovitskiy, A.; Beyer, L.; Kolesnikov, A.; Weissenborn, D.; Zhai, X.; Unterthiner, T.; Dehghani, M.; Minderer, M.; Heigold, G.; Gelly, S.; et al. 2020. An Image is Worth 16x16 Words: Transformers for Image Recognition at Scale. In *Proceedings of the International Conference on Learning Representations*, 1–12.
- Du, Z.; Li, J.; Su, H.; Zhu, L.; and Lu, K. 2021. Cross-domain gradient discrepancy minimization for unsupervised domain adaptation. In *Proceedings of the IEEE/CVF Conference on Computer Vision and Pattern Recognition*, 3937–3946.
- Feng, F.; Wang, J.; and Geng, X. 2024. Transferring Core Knowledge via Learngenes. *arXiv preprint arXiv:2401.08139*.
- Feng, F.; Wang, J.; Zhang, C.; Li, W.; Yang, X.; and Geng, X. 2023. Genes in Intelligent Agents. *arXiv preprint arXiv:2306.10225*.
- Feng, F.; Xie, Y.; Wang, J.; and Geng, X. 2024a. Redefining `!Creative!` in Dictionary: Towards a Enhanced Semantic Understanding of Creative Generation. *arXiv preprint arXiv:2410.24160*.
- Feng, F.; Xie, Y.; Wang, J.; and Geng, X. 2024b. Wave: Weight template for adaptive initialization of variable-sized models. *arXiv preprint arXiv:2406.17503*.
- Fu, Y.; Fu, Y.; and Jiang, Y.-G. 2021. Meta-fdmixup: Cross-domain few-shot learning guided by labeled target data. In *Proceedings of the ACM International Conference on Multimedia*, 5326–5334.
- Fu, Y.; Xie, Y.; Fu, Y.; Chen, J.; and Jiang, Y.-G. 2022. Me-d2n: Multi-expert domain decompositional network for cross-domain few-shot learning. In *Proceedings of the ACM International Conference on Multimedia*, 6609–6617.
- Fu, Y.; Xie, Y.; Fu, Y.; and Jiang, Y.-G. 2023. Styleadv: Meta style adversarial training for cross-domain few-shot learning. In *Proceedings of the IEEE/CVF Conference on Computer Vision and Pattern Recognition*, 24575–24584.
- Garcia, V.; and Bruna, J. 2018. Few-shot learning with graph neural networks. In *Proceedings of the International Conference on Learning Representations*, 1–12.
- Guo, Y.; Codella, N. C.; Karlinsky, L.; Codella, J. V.; Smith, J. R.; Saenko, K.; Rosing, T.; and Feris, R. 2020. A broader study of cross-domain few-shot learning. In *Proceedings of the European Conference on Computer Vision*, 124–141.
- He, K.; Zhang, X.; Ren, S.; and Sun, J. 2016. Deep residual learning for image recognition. In *Proceedings of the IEEE/CVF Conference on Computer Vision and Pattern Recognition*, 770–778.
- Helber, P.; Bischke, B.; Dengel, A.; and Borth, D. 2019. Eurosat: A novel dataset and deep learning benchmark for land use and land cover classification. *IEEE Journal of Selected Topics in Applied Earth Observations and Remote Sensing*, 12(7): 2217–2226.
- Hu, Y.; and Ma, A. J. 2022. Adversarial feature augmentation for cross-domain few-shot classification. In *Proceedings of the European Conference on Computer Vision*, 20–37.
- Islam, A.; Chen, C.-F. R.; Panda, R.; Karlinsky, L.; Feris, R.; and Radke, R. J. 2021. Dynamic distillation network for cross-domain few-shot recognition with unlabeled data. In *Proceedings of Advances in Neural Information Processing Systems*, 3584–3595.
- Kim, T.; and Han, B. 2024. Randomized adversarial style perturbations for domain generalization. In *Proceedings of the IEEE/CVF Winter Conference on Applications of Computer Vision*, 2317–2325.
- Krause, J.; Stark, M.; Deng, J.; and Fei-Fei, L. 2013. 3d object representations for fine-grained categorization. In *Proceedings of the IEEE/CVF International Conference on Computer Vision Workshops*, 554–561.
- Laenen, S.; and Bertinetto, L. 2021. On episodes, prototypical networks, and few-shot learning. In *Proceedings of Advances in Neural Information Processing Systems*, 24581–24592.
- Li, H.; Xu, Z.; Taylor, G.; Studer, C.; and Goldstein, T. 2018. Visualizing the loss landscape of neural nets. In *Proceedings of Advances in Neural Information Processing Systems*, 1–11.

- Li, L.; Xiao, J.; Chen, G.; Shao, J.; Zhuang, Y.; and Chen, L. 2024. Zero-shot visual relation detection via composite visual cues from large language models. In *Proceedings of Advances in Neural Information Processing Systems*.
- Li, P.; Gong, S.; Wang, C.; and Fu, Y. 2022a. Ranking distance calibration for cross-domain few-shot learning. In *Proceedings of the IEEE/CVF Conference on Computer Vision and Pattern Recognition*, 9099–9108.
- Li, X.; Dai, Y.; Ge, Y.; Liu, J.; Shan, Y.; and DUAN, L. 2022b. Uncertainty Modeling for Out-of-Distribution Generalization. In *International Conference on Learning Representations*, 1–13.
- Liang, H.; Zhang, Q.; Dai, P.; and Lu, J. 2021. Boosting the generalization capability in cross-domain few-shot learning via noise-enhanced supervised autoencoder. In *Proceedings of the IEEE/CVF International Conference on Computer Vision*, 9424–9434.
- Liu, B.; Zhao, Z.; Li, Z.; Jiang, J.; Guo, Y.; and Ye, J. 2020. Feature transformation ensemble model with batch spectral regularization for cross-domain few-shot classification. *arXiv preprint arXiv:2005.08463*.
- Mohanty, S. P.; Hughes, D. P.; and Salathé, M. 2016. Using deep learning for image-based plant disease detection. *Frontiers in Plant Science*, 7: 215232.
- Phoo, C. P.; and Hariharan, B. 2021. Self-training For Few-shot Transfer Across Extreme Task Differences. In *International Conference on Learning Representations*, 1–13.
- Qi, L.; Dong, P.; Xiong, T.; Xue, H.; and Geng, X. 2024. DoubleAUG: Single-domain Generalized Object Detector in Urban via Color Perturbation and Dual-style Memory. *ACM Transactions on Multimedia Computing, Communications and Applications*, 20(5): 1–20.
- Rame, A.; Dancette, C.; and Cord, M. 2022. Fishr: Invariant gradient variances for out-of-distribution generalization. In *Proceedings of the International Conference on Machine Learning*, 18347–18377.
- Ravi, S.; and Larochelle, H. 2017. Optimization as a model for few-shot learning. In *Proceedings of the International Conference on Learning Representations*, 1–11.
- Selvaraju, R. R.; Cogswell, M.; Das, A.; Vedantam, R.; Parikh, D.; and Batra, D. 2017. Grad-cam: Visual explanations from deep networks via gradient-based localization. In *Proceedings of the IEEE/CVF International Conference on Computer Vision*, 618–626.
- Snell, J.; Swersky, K.; and Zemel, R. 2017. Prototypical networks for few-shot learning. In *Proceedings of Advances in Neural Information Processing Systems*, volume 30.
- Sun, J.; Lopuschkin, S.; Samek, W.; Zhao, Y.; Cheung, N.-M.; and Binder, A. 2021. Explanation-guided training for cross-domain few-shot classification. In *Proceedings of the International Conference on Pattern Recognition*, 7609–7616.
- Sung, F.; Yang, Y.; Zhang, L.; Xiang, T.; Torr, P. H.; and Hospedales, T. M. 2018. Learning to compare: Relation network for few-shot learning. In *Proceedings of the IEEE/CVF Conference on Computer Vision and Pattern Recognition*, 1199–1208.
- Triantafyllou, E.; Zhu, T.; Dumoulin, V.; Lamblin, P.; Evci, U.; Xu, K.; Goroshin, R.; Gelada, C.; Swersky, K.; Manzagol, P.-A.; et al. 2020. Meta-Dataset: A Dataset of Datasets for Learning to Learn from Few Examples. In *International Conference on Learning Representations*, 1–13.
- Tschandl, P.; Rosendahl, C.; and Kittler, H. 2018. The HAM10000 dataset, a large collection of multi-source dermatoscopic images of common pigmented skin lesions. *Scientific Data*, 5(1): 1–9.
- Tseng, H.-Y.; Lee, H.-Y.; Huang, J.-B.; and Yang, M.-H. 2020. Cross-domain few-shot classification via learned feature-wise transformation. In *Proceedings of the International Conference on Learning Representations*, 1–14.
- Van Horn, G.; Mac Aodha, O.; Song, Y.; Cui, Y.; Sun, C.; Shepard, A.; Adam, H.; Perona, P.; and Belongie, S. 2018. The inaturalist species classification and detection dataset. In *Proceedings of the IEEE/CVF Conference on Computer Vision and Pattern Recognition*, 8769–8778.
- Wah, C.; Branson, S.; Welinder, P.; Perona, P.; and Belongie, S. 2011. The caltech-ucsd birds-200-2011 dataset.
- Wang, H.; and Deng, Z.-H. 2021. Cross-domain few-shot classification via adversarial task augmentation. In *Proceedings of the International Joint Conference on Artificial Intelligence*, 1075–1081.
- Wang, W.; Duan, L.; Wang, Y.; En, Q.; Fan, J.; and Zhang, Z. 2022. Remember the difference: Cross-domain few-shot semantic segmentation via meta-memory transfer. In *Proceedings of the IEEE/CVF Conference on Computer Vision and Pattern Recognition*, 7065–7074.
- Wang, X.; and He, K. 2021. Enhancing the transferability of adversarial attacks through variance tuning. In *Proceedings of the IEEE/CVF Conference on Computer Vision and Pattern Recognition*, 1924–1933.
- Wang, X.; Peng, Y.; Lu, L.; Lu, Z.; Bagheri, M.; and Summers, R. M. 2017. Chestx-ray8: Hospital-scale chest x-ray database and benchmarks on weakly-supervised classification and localization of common thorax diseases. In *Proceedings of the IEEE/CVF Conference on Computer Vision and Pattern Recognition*, 2097–2106.
- Xie, Y.; Feng, F.; Wang, J.; Geng, X.; and Rui, Y. 2024. Kind: Knowledge integration and diversion in diffusion models. *arXiv preprint arXiv:2408.07337*.
- Yu, T.; Kumar, S.; Gupta, A.; Levine, S.; Hausman, K.; and Finn, C. 2020. Gradient surgery for multi-task learning. In *Proceedings of Advances in Neural Information Processing Systems*, 5824–5836.
- Zhang, J.; Song, J.; Gao, L.; and Shen, H. 2022. Free-lunch for cross-domain few-shot learning: Style-aware episodic training with robust contrastive learning. In *Proceedings of the ACM International Conference on Multimedia*, 2586–2594.
- Zhang, X.; Xu, R.; Yu, H.; Zou, H.; and Cui, P. 2023. Gradient norm aware minimization seeks first-order flatness and improves generalization. In *Proceedings of the IEEE/CVF Conference on Computer Vision and Pattern Recognition*, 20247–20257.

- ZHENG, H.; Wang, R.; Liu, J.; and Kanazaki, A. 2023. Cross-Level Distillation and Feature Denoising for Cross-Domain Few-Shot Classification. In *Proceedings of the International Conference on Learning Representations*, 1–12.
- Zhong, Z.; Zhao, Y.; Lee, G. H.; and Sebe, N. 2022. Adversarial style augmentation for domain generalized urban-scene segmentation. *Advances in Neural Information Processing Systems*, 35: 338–350.
- Zhou, B.; Lapedriza, A.; Khosla, A.; Oliva, A.; and Torralba, A. 2017. Places: A 10 million image database for scene recognition. *IEEE Transactions on Pattern Analysis and Machine Intelligence*, 40(6): 1452–1464.
- Zhou, F.; Wang, P.; Zhang, L.; Wei, W.; and Zhang, Y. 2023. Revisiting prototypical network for cross domain few-shot learning. In *Proceedings of the IEEE/CVF Conference on Computer Vision and Pattern Recognition*, 20061–20070.
- Zhou, K.; Yang, Y.; Qiao, Y.; and Xiang, T. 2020. Domain Generalization with MixStyle. In *Proceedings of the International Conference on Learning Representations*, 1–12.
- Zhuo, L.; Fu, Y.; Chen, J.; Cao, Y.; and Jiang, Y.-G. 2022. Tgdm: Target guided dynamic mixup for cross-domain few-shot learning. In *Proceedings of the ACM International Conference on Multimedia*, 6368–6376.
- Zou, Y.; Liu, Y.; Hu, Y.; Li, Y.; and Li, R. 2024. Flatten Long-Range Loss Landscapes for Cross-Domain Few-Shot Learning. In *Proceedings of the IEEE/CVF Conference on Computer Vision and Pattern Recognition*, 23575–23584.

Supplementary Material for “SVasP: Self-Versatility Adversarial Style Perturbation for Cross-Domain Few-Shot Learning”

In the supplementary material, we provide:

- More implementation details of the proposed methods.
- More experimental results of ablation studies.
- More visualization results for model evaluation.

A. More Implementation Details

A.1. Model-Based Style Generation.

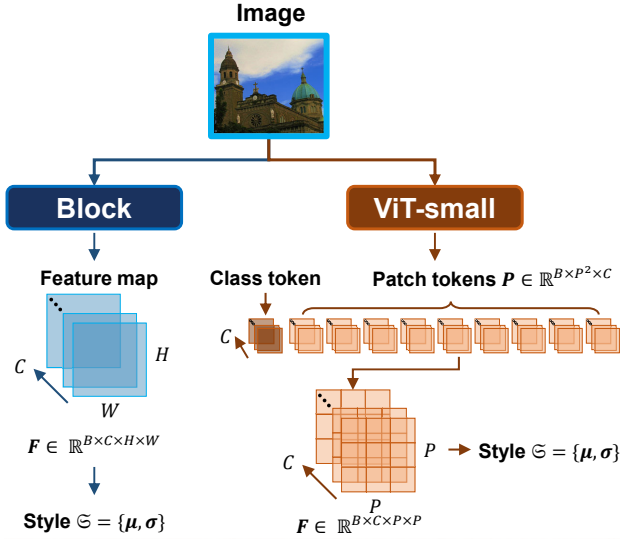


Figure 8: Comparison of style generation methods for different backbones.

The main basis of our approach is to represent the style of the domain, in addition our experiments involved two different backbones, so we detail the style generation mechanism for the different backbones.

Specifically, for the ResNet-10 backbone, styles of four blocks’ features are generated for iterative adversarial style generation, separately. For each block, We get the feature map $F \in \mathbb{R}^{B \times C \times H \times W}$, where B, C, H and W denote the batch size, channel, height, width of the feature maps F .

For the ViT-small backbone, the input goes through the ViT-small backbone and outputs class tokens and patch tokens P , we ignore class tokens and use only patch tokens P . We then reshape the patch tokens $P \in \mathbb{R}^{B \times P^2 \times C}$ into the feature map $F \in \mathbb{R}^{B \times C \times H \times W}$, where $H = W = P$.

At this point, we get the corresponding feature maps F for the two backbones, as shown in Figure 8. Thus, we can get the style $\mathfrak{S} = \{\mu, \sigma\}$ by the equations:

$$\mu = \frac{1}{HW} \sum_{h=1}^H \sum_{w=1}^W F_{B,C,h,w}, \quad (22)$$

$$\sigma = \sqrt{\frac{1}{HW} \sum_{h=1}^H \sum_{w=1}^W (F_{B,C,h,w} - \mu)^2 + \epsilon}, \quad (23)$$

where ϵ is a small value to avoid division by zero.

Algorithm 1: SVasP attack method

Input: Benign image x , target label y , backbone E with four blocks $\{B_j\}_{j=1}^4$, standard cross-entropy loss $\mathcal{L}_{CE}(\cdot, \cdot)$.

Parameter: Scale parameter $s = \{s_l, s_h\}$, decay factor ξ , attack parameter κ_1 and κ_2 .

Output: Adversarial style set $\mathbb{S}_{adv} = \{\mathfrak{S}_{adv}^1, \mathfrak{S}_{adv}^2, \mathfrak{S}_{adv}^3\}$.

- 1: Random crop and resize k crop images of x and get the input set: $\mathbb{I} = \{c_1, c_2, \dots, c_k, x\}$.
 - 2: **for** $j = 1$ to 3 **do**
 - 3: **for** I in \mathbb{I} **do**
 - 4: $F = \mathfrak{T}_j(\mathfrak{T}_{j-1}(\dots(\mathfrak{T}_1(I, \mathfrak{S}_{adv}^1), \dots), \mathfrak{S}_{adv}^{j-1}), \mathfrak{S}_{adv}^j)$
 - 5: Calculate the style $\mathfrak{S} = \{\mu, \sigma\}$ of F by Eq.(22), (23)
 - 6: Get the prediction $p = f_g(B_4(\dots(B_{j+1}(F)))$; θ_g)
 - 7: $\mathcal{L}_{std} = \mathcal{L}_{std} + \mathcal{L}_{CE}(p, y)$
 - 8: Calculate the style gradient $\{\nabla_{\mu} \mathcal{L}_{std}, \nabla_{\sigma} \mathcal{L}_{std}\}$
 - 9: **end for**
 - 10: Get the total style gradient set by Eq. (24) and (25).
 - 11: Get the aggregated crop style gradients by Eq. (26) and (27).
 - 12: Get the ensemble style gradients by Eq.(28) and (29).
 - 13: Get the adversarial styles of B_j by Eq. (30), (31), (32) and (33).
 - 14: **end for**
 - 15: **return** $\mu_{adv}^1, \sigma_{adv}^1, \mu_{adv}^2, \sigma_{adv}^2, \mu_{adv}^3, \sigma_{adv}^3$
-

A.2. Self-Versatility Gradient Ensemble Perturbation.

One of our key contributions is the ensemble of the style gradients of crop images with the image itself, which we called self-versatility. To better help understand our proposed method, we compare it with the vanilla global style perturbation method, as illustrated in Figure 9. The direct vanilla global style perturbation methods produce more homogeneous styles, and the use of source domain style gradients is not maximized, limiting style diversity. In contrast, our proposed method covers more information about the style of the source domain, which makes the generated adversarial style more domain-independent and generalizable.

Moreover, as iterative synthesizing strategy is confirmed to be effective in style attack, we present the novel SVasP adversarial training method progressively. The complete adversarial style generation pseudo-code is shown in Algorithm 1. The formulas used in the pseudo-code are listed below:

$$\begin{aligned} \mathbb{G}^{\mu} &= \{\mathcal{G}_1^{\mu}, \mathcal{G}_2^{\mu}, \dots, \mathcal{G}_k^{\mu}, \mathcal{G}_g^{\mu}\} \\ &= \{\nabla_{\mu_1} \mathcal{L}_{std}, \nabla_{\mu_2} \mathcal{L}_{std}, \dots, \nabla_{\mu_k} \mathcal{L}_{std}, \nabla_{\mu_g} \mathcal{L}_{std}\} \end{aligned} \quad (24)$$

$$\begin{aligned} \mathbb{G}^{\sigma} &= \{\mathcal{G}_1^{\sigma}, \mathcal{G}_2^{\sigma}, \dots, \mathcal{G}_k^{\sigma}, \mathcal{G}_g^{\sigma}\} \\ &= \{\nabla_{\sigma_1} \mathcal{L}_{std}, \nabla_{\sigma_2} \mathcal{L}_{std}, \dots, \nabla_{\sigma_k} \mathcal{L}_{std}, \nabla_{\sigma_g} \mathcal{L}_{std}\} \end{aligned} \quad (25)$$

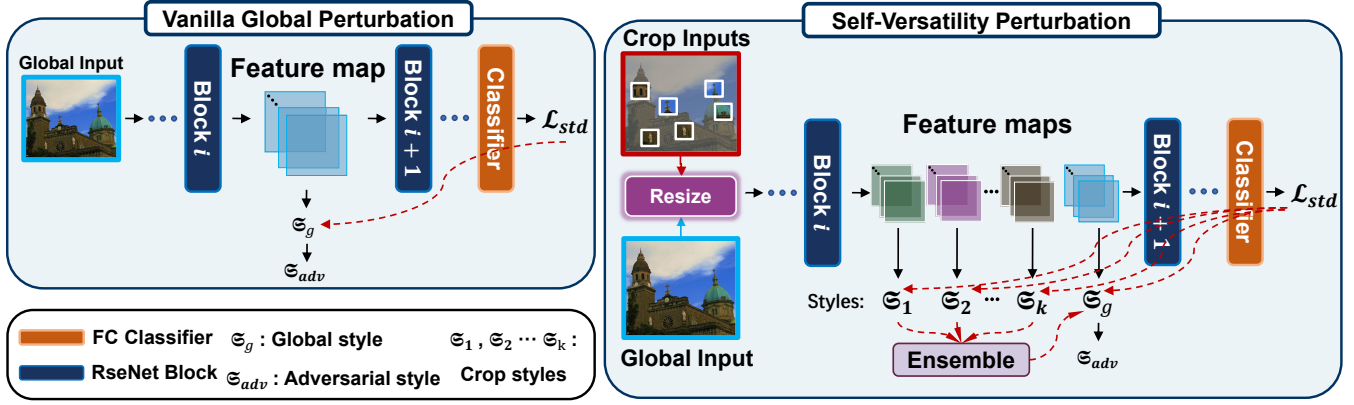


Figure 9: Comparison of the vanilla global perturbation and our self-versatility perturbation methods.

$$\mathcal{G}_c^\mu = \text{Norm}\left(\frac{1}{k} \sum (\mathcal{G}_1^\mu + \mathcal{G}_2^\mu + \dots + \mathcal{G}_k^\mu)\right) \quad (26)$$

$$\mathcal{G}_c^\sigma = \text{Norm}\left(\frac{1}{k} \sum (\mathcal{G}_1^\sigma + \mathcal{G}_2^\sigma + \dots + \mathcal{G}_k^\sigma)\right) \quad (27)$$

$$\mathcal{G}_e^\mu = \text{Norm}(\mathcal{G}_g^\mu) + \xi \odot \mathcal{G}_c^\mu \quad (28)$$

$$\mathcal{G}_e^\sigma = \text{Norm}(\mathcal{G}_g^\sigma) + \xi \odot \mathcal{G}_c^\sigma \quad (29)$$

$$\boldsymbol{\mu}_{init} = \boldsymbol{\mu}_g + \varepsilon \cdot \mathcal{N}(0, I) \quad (30)$$

$$\boldsymbol{\sigma}_{init} = \boldsymbol{\sigma}_g + \varepsilon \cdot \mathcal{N}(0, I) \quad (31)$$

$$\boldsymbol{\mu}_{adv} = \boldsymbol{\mu}_{init} + \kappa_1 \cdot \text{sign}(\mathcal{G}_e^\mu) \quad (32)$$

$$\boldsymbol{\sigma}_{adv} = \boldsymbol{\sigma}_{init} + \kappa_2 \cdot \text{sign}(\mathcal{G}_e^\sigma) \quad (33)$$

A.3. More Details for DCO.

Given the clean inputs and the adversarial features after perturbation, DCO consists of three sub losses: the domain discrepancy loss \mathcal{L}_{dom} , the global-crop consistency loss \mathcal{L}_{con} and the global-adversarial consistency loss \mathcal{L}_{adv} .

Domain Discrepancy Loss. The \mathcal{L}_{dom} is introduced to distinguish between seen and unseen domains to keep the adversarial style as far away from the source domain restrictions as possible. For global and crop features, they are all classified to the seen domain and thus their domain labels d_F are all 0. Besides, our main goal is to make the generated adversarial features more migratory and more unseen domain in nature, so we classify them to the unseen domain with domain labels $d_F = 1$. Thus, the domain discriminator in the module is a binary header, consisting of one fully connected layer. For each final feature passed through the backbone $\mathbf{F} \in \mathbb{R}^{B \times C}$, we can get the domain prediction $\mathbf{p}_{dom} = f_{dom}(\mathbf{F}; \theta_{dom})$, where $\mathbf{p}_{dom} \in \mathbb{R}^{B \times 2}$. Thus, we can get:

$$\mathcal{L}_{dom} = \mathcal{L}_{CE}(\mathbf{p}_{dom}, d_F) \quad (34)$$

Crop Consistency Loss. The \mathcal{L}_{con} is introduced to restrict crop inputs. On one hand, crop and global prediction need to be semantically unified. Specifically, for the k crop images, the global-crop consistency loss can be calculated by the following equation:

$$\mathcal{L}_{cg} = \sum_{i=1}^k \mathcal{L}_{CE}(\mathbf{p}_i, \mathbf{p}_g) \quad (35)$$

On the other hand, crop inputs need to achieve N -way K -shot Few-shot classification. Instead of using the benign labels, meta-learning adopts N -way K -shot logical labels. Specifically, for the image which belongs to the i class of the N classes, the N -way K -shot logical label of the image is set as y_{ws} . Since we random crop the global images while preserve the semantics, the crop images still belong to the same logic label. Thus, the N -way K -shot loss for crop inputs is defined as:

$$\mathcal{L}_c^{ws} = \sum_{i=1}^k \mathcal{L}_{CE}(\mathbf{p}_i, y_{ws}) \quad (36)$$

Then, we can get the final crop consistency loss with the hyper-parameter λ :

$$\begin{aligned} \mathcal{L}_{con} &= \lambda \mathcal{L}_{cg} + (1 - \lambda) \mathcal{L}_c^{ws} \\ &= \sum_{i=1}^k (\lambda \mathcal{L}_{CE}(\mathbf{p}_i, \mathbf{p}_g) + (1 - \lambda) \mathcal{L}_{CE}(\mathbf{p}_i^{ws}, y_{ws})) \end{aligned} \quad (37)$$

Global-Adversarial Consistency Loss. The \mathcal{L}_{adv} is introduced to constrain the prediction \mathbf{p}_{adv}^{ws} and \mathbf{p}_g^{ws} by the Kullback-Leibler divergence loss, which is calculated by:

$$\mathcal{L}_{adv} = \frac{1}{NM * N} \sum_{i=1}^{NM} \sum_{j=1}^N \mathbf{p}_{g_{ij}}^{ws} * \log \frac{\mathbf{p}_{g_{ij}}^{ws}}{\mathbf{p}_{adv_{ij}}^{ws}} \quad (38)$$

A.4. Details for Benchmarks and Datasets.

The BSCD-FSL benchmark is proposed in BSCD-FSL (Guo et al. 2020) and the *mini*-CUB benchmark is proposed in FWT (Tseng et al. 2020). BSCD-FSL (Guo et al. 2020) benchmark: Broader Study of Cross-Domain Few-Shot Learning (BSCD-FSL) benchmark includes image data from a diverse assortment of image acquisition methods. There are five datasets which are *mini*ImageNet (Ravi and Larochelle 2017), ChestX (Wang et al. 2017), ISIC (Tschandl, Rosendahl, and Kittler 2018), EuroSAT (Helber et al. 2019) and CropDiseases (Mohanty, Hughes, and Salathé 2016).

- *mini*ImageNet (Ravi and Larochelle 2017): A dataset consists of 60000 images in total, evenly distributed across 100 classes.

- ChestX (Wang et al. 2017): A medical imaging dataset which comprises 108,948 frontal-view X-ray images of 32,717 unique patients with the text-mined eight disease image labels.
- ISIC (Tschandl, Rosendahl, and Kittler 2018): A dataset published by the International Skin Imaging Collaboration as a large-scale dataset of dermoscopy images.
- EuroSAT (Helber et al. 2019): A dataset based on Sentinel-2 satellite images covering 13 spectral bands and consisting out of 10 classes.
- CropDiseases (Mohanty, Hughes, and Salathé 2016): A dataset consists of about 87K RGB images of healthy and diseased crop leaves which is categorized into 38 different classes.

mini-CUB (Tseng et al. 2020): *mini-CUB* benchmark is proposed in FWT (Tseng et al. 2020), including five datasets which are *miniImageNet* (Ravi and Larochelle 2017), CUB (Wah et al. 2011), Cars (Krause et al. 2013), Places (Zhou et al. 2017) and Plantae (Van Horn et al. 2018). In this benchmark, *miniImageNet* is always regarded as the source domain and others datasets are regarded as the target domains.

- CUB (Wah et al. 2011): A dataset contains 200 different categories of bird images.
- Cars (Krause et al. 2013): The Stanford Cars dataset consists of 196 classes of cars with a total of 16,185 images.
- Places (Zhou et al. 2017): A dataset contains over 10 millions labeled exemplars from 434 place categories.
- Plantae (Van Horn et al. 2018): Plantae dataset is one of dataset iNat2017. There are 2101 categories and 196613 images in this dataset.

A.5. Details for Finetuning.

We follow the finetune setting in StyleAdv (Fu et al. 2023) to ensure that the comparison is fair. Specifically, we finetune the meta-trained model with pseudo training episodes. The specific finetuning details are shown in Table 4. Compared with 5-way 1-shot tasks, 5-way 5-shot tasks need more training iterations because more query images are required to be classified. Compared with ResNet-10 backbone, ViT-small backbone need smaller learning rate because ViT-small model are pretrained on the large-scale model.

| Backbone | Task | Opt. | Iter. | lr |
|-----------|--------------|------|-------|------------|
| ResNet-10 | 5-way 1-shot | Adam | 10 | {0, 0.005} |
| ResNet-10 | 5-way 5-shot | Adam | 50 | {0, 0.001} |
| ViT-small | 5-way 1-shot | SGD | 20 | {0, 5e-5} |
| ViT-small | 5-way 5-shot | SGD | 50 | {0, 5e-5} |

Table 4: The finetuning details for ResNet-10 and ViT-small backbones. The ‘‘Opt.’’, the ‘‘Iter.’’ and the ‘‘lr’’ represent the optimizer, the finetuning iterations and the learning rate, respectively.

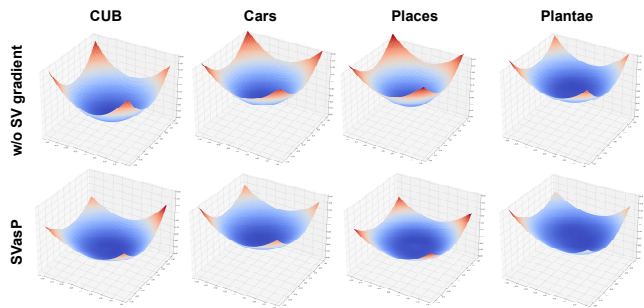


Figure 10: Loss landscape visualization results of the model without SV gradient ensemble module (first row) and our SVasP model (second row) on the *mini-CUB* benchmark.



Figure 11: Grad-CAM visualization results of the StyleAdv model and our SVasP model on the *mini-CUB* benchmark. For each target dataset, three examples are demonstrated.

B. More Experimental Results

B.1. Impact of different crop numbers k .

The results of the experiments on each dataset for different number of crops k are shown in Table 8. From the experimental results on each dataset, it can be seen that the optimal classification accuracy is achieved regardless of any dataset when $k = 2$. Setting k to 2 is the optimal solution, which can effectively improve the generalization of the model and will not lead to model overfitting.

B.2. Impact of different strategies for ξ and λ .

The results of the experiments on each dataset for different values of ξ are shown in Table 5. As can be seen from the table, when $\xi = 0.1$, a significant performance improvement is realized compared to the other set values, regardless of the dataset. In addition, the results of the experiments for different values of λ are shown in Table 6. The optimal classification accuracy is achieved only on the Places dataset by setting the value of λ to 1. On the rest of the datasets, optimal classification accuracy is achieved when the value of λ is set to 0.2.

B.3. Impact of different selection methods for κ_1 and κ_2 .

The results of the experiments on each dataset for whether setting κ_1 and κ_2 to the same value are shown in Table 7. From the results in the table, it can be seen that not restricting κ_1 and κ_2 to the same value can effectively increase the

| ξ | ChestX | ISIC | EuroSAT | CropDisease | CUB | Cars | Places | Plantae | Aver. |
|-------------------|-------------------|-------------------|-------------------|-------------------|-------------------|-------------------|-------------------|-------------------|--------------|
| 0 | 25.33±0.36 | 48.92±0.55 | 87.17±0.53 | 93.36±0.41 | 64.84±0.70 | 49.29±0.65 | 76.02±0.62 | 57.24±0.66 | 62.77 |
| 0.01 | 25.32±0.36 | 47.81±0.54 | 86.88±0.56 | 92.55±0.44 | 66.12±0.69 | 48.53±0.67 | 75.92±0.65 | 58.18±0.65 | 62.66 |
| 0.1 (Ours) | 26.87±0.38 | 51.10±0.58 | 88.72±0.52 | 94.52±0.33 | 68.95±0.66 | 52.13±0.66 | 77.78±0.62 | 60.63±0.64 | 65.09 |
| 1 | 26.65±0.39 | 49.62±0.55 | 86.17±0.53 | 91.07±0.47 | 67.13±0.66 | 51.30±0.69 | 77.22±0.62 | 58.18±0.65 | 63.42 |

Table 5: More specific results on different decay factors for ξ . The accuracy (%) with RseNet-10 and GNN under the 5-way 5-shot setting is reported. “**Aver.**” means “Average Accuracy” of the eight datasets. The optimal results are marked in **bold**.

| λ | ChestX | ISIC | EuroSAT | CropDisease | CUB | Cars | Places | Plantae | Aver. |
|-------------------|-------------------|-------------------|-------------------|-------------------|-------------------|-------------------|-------------------|-------------------|--------------|
| 0 | 26.40±0.38 | 49.62±0.55 | 87.31±0.53 | 93.47±0.42 | 67.86±0.69 | 51.30±0.69 | 76.89±0.62 | 57.48±0.65 | 63.79 |
| 0.2 (Ours) | 26.87±0.38 | 51.10±0.58 | 88.72±0.52 | 94.52±0.33 | 68.95±0.66 | 52.13±0.66 | 77.78±0.62 | 60.63±0.64 | 65.09 |
| 0.5 | 26.09±0.36 | 49.23±0.53 | 88.03±0.52 | 92.67±0.42 | 67.91±0.67 | 50.07±0.66 | 76.95±0.62 | 58.54±0.67 | 63.69 |
| 0.8 | 25.61±0.37 | 49.03±0.53 | 87.35±0.51 | 93.34±0.40 | 65.53±0.68 | 49.62±0.63 | 75.58±0.64 | 58.32±0.63 | 62.72 |
| 1 | 26.18±0.38 | 49.46±0.54 | 87.05±0.55 | 92.46±0.43 | 67.26±0.67 | 50.47±0.68 | 77.84±0.61 | 59.40±0.66 | 63.67 |

Table 6: More specific results on different crop consistency loss functions with different strategies for λ . The accuracy (%) with RseNet-10 and GNN under the 5-way 5-shot setting is reported. “**Aver.**” means “Average Accuracy” of the eight datasets. The optimal results are marked in **bold**.

| $\kappa_1 \kappa_2$ | ChestX | ISIC | EuroSAT | CropDisease | CUB | Cars | Places | plantae | Average |
|---------------------|-------------------|-------------------|-------------------|-------------------|-------------------|-------------------|------------|-------------------|--------------|
| Baseline | 26.21±0.31 | 49.99±0.61 | 88.23±0.53 | 93.89±0.32 | 66.49±0.69 | 51.91±0.68 | 75.01±0.64 | 59.20±0.65 | 63.87 |
| Ours | 26.87±0.38 | 51.10±0.58 | 88.72±0.52 | 94.52±0.33 | 68.95±0.66 | 52.13±0.66 | 77.78±0.62 | 60.63±0.64 | 65.09 |

Table 7: More specific results on different selection methods for κ_1 and κ_2 . The accuracy (%) with RseNet-10 and GNN under the 5-way 5-shot setting is reported. “**Aver.**” means “Average Accuracy” of the eight datasets.

| k | ChestX | ISIC | EuroSAT | CropDisease | CUB | Cars | Places | plantae |
|-----------------|-------------------|-------------------|-------------------|-------------------|-------------------|-------------------|-------------------|-------------------|
| 0 | 26.23±0.37 | 47.34±0.55 | 86.38±0.54 | 91.71±0.44 | 64.98±0.67 | 47.78±0.64 | 75.58±0.61 | 58.27±0.66 |
| 1 | 25.31±0.37 | 49.26±0.53 | 87.17±0.53 | 93.36±0.41 | 66.18±0.67 | 49.99±0.65 | 76.02±0.62 | 57.32±0.64 |
| 2 (Ours) | 26.87±0.38 | 51.10±0.58 | 88.72±0.52 | 94.52±0.33 | 68.95±0.66 | 52.13±0.66 | 77.78±0.62 | 60.63±0.64 |
| 3 | 25.46±0.35 | 47.69±0.53 | 88.03±0.52 | 92.99±0.42 | 65.72±0.70 | 50.39±0.66 | 76.85±0.61 | 58.90±0.66 |
| 4 | 25.59±0.37 | 49.59±0.53 | 87.92±0.50 | 94.01±0.38 | 64.84±0.66 | 50.16±0.67 | 75.31±0.64 | 57.66±0.65 |
| 5 | 24.94±0.35 | 48.21±0.52 | 86.54±0.51 | 92.19±0.44 | 62.76±0.69 | 49.17±0.62 | 74.88±0.63 | 55.00±0.63 |

Table 8: More specific results on crop numbers k . The accuracy (%) with RseNet-10 and GNN under the 5-way 5-shot setting is reported. “**Aver.**” means “Average Accuracy” of the eight datasets.

accuracy. This is because varying κ_1 and κ_2 by different magnitudes can simulate a wider variety of styles, enhancing generalization.

C. More Visualization Results

C.1. Loss Landscape Visualization Results.

We complement the loss landscape visualization results on the *mini-CUB* benchmark, as shown in Figure 10. Consistent with experimental results on the BSCD-FSL benchmark, our proposed method SVasP achieves flatter loss landscape near the optimum that our model converges on.

C.2. Grad-CAM Visualization Results.

We also complement Grad-CAM visualization results on the *mini-CUB* benchmark, as shown in Figure 11.